INTERNATIONAL JOURNAL FOR NUMERICAL METHODS IN FLUIDS
Int. J. Numer. Meth. Fluids 2002; **38**:895–917 (DOI: 10.1002/fld.254)

The effect of solutal undercooling on double-diffusive convection and macrosegregation during binary alloy solidification: a numerical investigation

Suman Chakraborty[1,†] and Pradip Dutta[2,*,‡]

[1] *Department of Power Plant Engineering, Jadavpur University, Calcutta-700091, India*
[2] *Department of Mechanical Engineering, Indian Institute of Science, Bangalore-560012, India*

SUMMARY

In this paper, we present a macroscopic numerical model that is capable of capturing the interaction between the double-diffusive convective field and a localized fluid flow on account of solutal undercooling during non-equilibrium solidification of binary alloys. The model is essentially based on a fixed-grid enthalpy based control volume approach. In the present model, microscopic features pertaining to non-equilibrium effects on account of solutal undercooling are incorporated through the formulation of a modified partition-coefficient. The effective partition-coefficient is numerically modelled by means of a number of macroscopically observable parameters related to the solidifying domain. This feature has made the present treatment different from micro–macro modelling of alloy solidification, which involves certain parameters that may not be macroscopically resolvable. Numerical simulations are performed for the case of two-dimensional transient solidification of Pb–Sn alloys (both hypoeutectic and hypereutectic) in a rectangular cavity, employing the present model. The simulation results are also compared with the corresponding experimental results quoted in the literature, and the agreement is excellent. From the results, it can be concluded that non-equilibrium effects on account of solutal undercooling result in a more enhanced macrosegregation. Copyright © 2002 John Wiley & Sons, Ltd.

KEY WORDS: macroscopic; solutal undercooling; double-diffusive convection; modification of partition-coefficient; macrosegregation

1. INTRODUCTION

The freezing of a solid from a melt involves numerous complex physical issues, many of which are closely associated with the fluid flow that accompanies the phase-transition process during solidification. For instance, when an alloy solidifies, the morphology often takes the form of dendrites, which reject solute throughout the 'mushy' zone and into a diffusion

* Correspondence to: P. Dutta, Department of Mechanical Engineering, Indian Institute of Science, Bangalore-560012, India.
† E-mail: sumanc@mecheng.iisc.ernet.in
‡ E-mail: pradip@mecheng.iisc.ernet.in

Received 22 November 2000
Revised 28 May 2001

layer ahead of the dendritic front. The melt, in turn, interacts with the mush and its diffusion layer both solutally and thermally, resulting in a situation where both temperature and solute concentration gradients play significant roles. The temperature gradients arise from externally imposed boundary conditions as well as evolution of latent heat within the mushy region. The concentration gradients, on the other hand, are caused by the rejection of solute at the solid/liquid interface, and transport of solute by diffusion and convection in the liquid region. These two gradients lead to a fluid flow on account of thermal and solutal buoyancy in both mushy and liquid regions, the resulting flow being known as double-diffusive convection. This thermo–solutal convection may result in a composition variation over distances comparable to the size of the solidification domain due to transport of rejected solute with fluid flow further away from the freezing boundary, the phenomenon being known as macrosegregation.

Numerous computational studies have been undertaken to examine the inter-relationship between double-diffusive convection and dendritic solidification. The most important finding of these studies [1–3] is that double diffusive convection plays an important role in the long-range transport of solute and thereby controls the final macrosegregation pattern. This has given rise to a major challenge in the field of macroscopic modelling of solidification, by emphasizing the need for proper accounting of microscopic issues that dictate the final macrosegregation behaviour through double-diffusive convection.

While reviewing literature on modelling of dendritic solidification systems, a clear distinction needs to be made regarding the microscopic and macroscopic approaches. The microscopic approach essentially deals with length scales of the same order as that of the dendrite arms [4–12]. In this manuscript, we choose to highlight only some of the landmark investigations (pertaining to micro-modelling) relevant to the present context. In general, the classical non-equilibrium freezing equation given by Scheils model [13] has been used widely for predicting microscopic solute redistribution between dendrite arms, provided diffusion in the solid can be neglected. As an improvement to this model, Brody and Flemings [4] presented an analytical expression to account for diffusion in the solid. The model is capable of predicting final solute redistribution after solidification and cooling to room temperature and local fraction of solid as a function of temperature within the solidifying domain. The analysis has been based on the assumption of negligible undercooling before nucleation of solid phases. The above model does not conserve solute [5] and might lead to incorrect predictions when solid-state diffusion is finite. Clyne and Kurz [5] presented a modification of the above model for a more accurate prediction of microsegregation profiles in binary alloys. Ohanka [6] analysed the solute distribution during solidification by a profile method, which provided a better estimate of microsegregation than the Brody–Flemings equation. Kobayashi [7] presented the exact solution of the microsegregation model proposed by Brody and Flemings [4] under the conditions of constant equilibrium partition-ratio, constant diffusion coefficient of solute in the solid, and parabolic growth. It can be noted here that all the above models of solidification essentially neglected solutal undercooling effects during the solidification process.

Incorporation of solutal undercooling effects in solidification modelling has subsequently been initiated through ‘micro–macro modelling’ [14], where the aim has been the prediction of microstructure using microscopic growth and nucleation models. Since these models require cooling rate as an input, appropriate cooling rates are predicted from a macroscopic heat transfer model. In such a micro–macro model, Rappaz [14] accounted for solutal undercooling through a kinetic law for calculation of solid volume fraction in the latent heat release source

terms, neglecting convection effects in the liquid. Nevertheless, many of the microscopic and macro–micro models have been effectively used to develop fundamental understanding of species transport mechanisms during dendritic solidification of binary alloy systems.

However, very often, for prediction of large-scale features such as macrosegregation, macroscale models [1–3] for predicting momentum, heat and solute transport mechanisms are invoked. In such models, one may note that macroscopic solidification events are strongly influenced by microscopic phenomena, and hence consistent representation of appropriate microscopic behaviour needs to be adopted within the framework of the macroscopic model. Although effects of solutal undercooling have been extensively analysed in microscopic solidification models [15], such considerations in the context of macroscopic numerical modelling of alloy solidification have been missing. Incorporation of such effects may involve certain macroscopically-irresolvable parameters (such as characteristic diameter of crystals, nucleation rate, and grain radius), thus providing a challenge in their numerical implementation in a macroscopic framework.

In the present numerical study, we attempt to devise a macroscopic mathematical model that accounts for solutal undercooling during binary alloy solidification, through a correction of the partition-coefficient. This approach is different from the previous attempts on modelling of solutal undercooling in a microscopic framework, as given in the literature cited above. The modified partition-coefficient is described in terms of macroscopically resolvable parameters pertaining to the solidifying domain. Such a modification of partition-coefficient is eventually correlated with the double-diffusive convection field so that the final macrosegregation behaviour can be effectively predicted. As a demonstration of the numerical model developed in this study, we simulate the directional solidification of Pb–Sn alloys in a rectangular cavity, corresponding to both hypoeutectic and hypereutectic initial composition of the alloy. The selection of the corresponding initial alloy compositions is made in such a way that they result in two distinct types of thermo–solutal convection patterns. This double-diffusive flow-field, in turn, is expected to control the species redistribution throughout the solidifying domain, where solute build-up ahead of the phase-changing front (i.e. solutal undercooling) is likely to become significant. The numerical predictions regarding the same are then compared with the macrosegregation patterns obtained from corresponding experimental work reported in the literature [16]. We compare the experimental results with the numerical predictions with and without the solutal undercooling model. Such a comparison is expected to reveal the importance of incorporation of solutal undercooling in numerical schemes, in terms of accurate prediction of the final macrosegregation pattern.

2. MATHEMATICAL MODELLING

2.1. The physical problem

The present work investigates the solidification of a binary alloy in a rectangular domain, with the vertical boundaries subjected to prescribed temperature conditions, and the horizontal boundaries kept insulated. The melt, with an initial superheat, is poured into the cavity, where it starts solidifying from a vertical boundary. The problem domain is shown schematically in Figure (1), depicting the initial and boundary conditions.

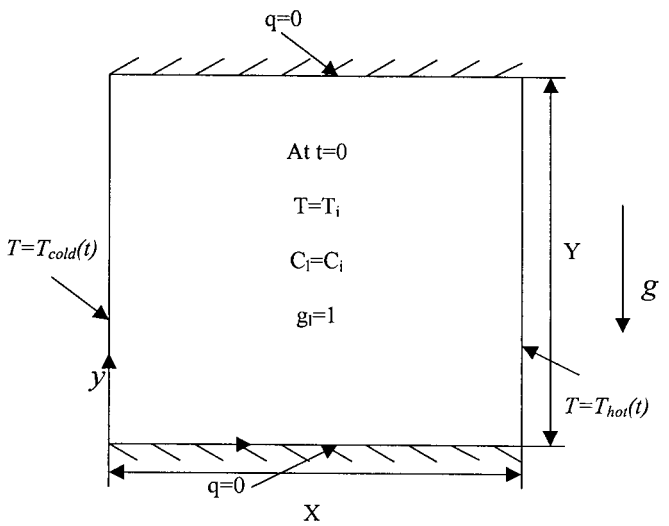

Figure 1. Problem domain with initial and boundary conditions.

2.2. *The conservation equations*

By employing a single-domain continuum formulation with appropriate volume averaging of individual phase equations, macroscopic conservation equations for mass, momentum, energy and species conservation can be written. The details of the formulation can be found in Voller *et al.* [3], and are not discussed here in detail for the purpose of brevity.

$$\text{Continuity:}\quad \frac{\partial}{\partial t}(\rho) + \nabla \cdot (\rho \vec{u}) = 0 \tag{1}$$

$$x\text{-momentum:}\quad \frac{\partial}{\partial t}(\rho u) + \nabla \cdot (\rho \vec{u} u) = \nabla \cdot \left(\mu_{\mathrm{l}} \frac{\rho}{\rho_{\mathrm{l}}} \nabla u\right) - \frac{\partial p}{\partial x} + S_u \tag{2}$$

$$y(\text{vertical})\text{-momentum:}\quad \frac{\partial}{\partial t}(\rho v) + \nabla \cdot (\rho \vec{u} v) = \nabla \cdot \left(\mu_{\mathrm{l}} \frac{\rho}{\rho_{\mathrm{l}}} \nabla v\right) - \frac{\partial p}{\partial y} + S_v + S_b \tag{3}$$

where

$$S_b = \rho_{\mathrm{ref}} g[\beta_{\mathrm{T}}(T - T_{\mathrm{ref}}) + \beta_{\mathrm{S}}(C_{\mathrm{l}} - C_{\mathrm{ref}})] \tag{3a}$$

Consistent with the physics of dendritic growth, the source terms S_u and S_v are evaluated from Darcy's model of viscous flow through a porous medium (assuming zero velocity of solid phase and isotropic permeability) as

$$S_{\mathrm{i}} = -\frac{\mu_{\mathrm{l}} \rho u_{\mathrm{i}}}{K \rho_{\mathrm{l}}} \tag{4}$$

where u_{i} represents the speed in appropriate direction and K is a porosity constant. For appropriate modelling of the above term, K has to be properly prescribed as a function of

liquid fraction. For that purpose, the Carman–Kozeny relation is used within a range of validity of $0 < g_l < 0.5$; i.e.

$$K = K_0 \frac{g_l^3}{(1 - g_l)^2} \tag{5}$$

However, due to inaccuracy of this equation for $g_l > 0.5$, a hybrid model is used for that region [17] as given by

$$\mu_l = \mu_l^0 \left(\frac{A_\mu}{A_\mu - F g_s} \right)^2 \tag{6}$$

$$K = G K_0 \left[\frac{g_l^3}{(1 - g_l)^2} \right] \quad \text{where } A_\mu = 0.4 \tag{7}$$

Here, F and G are according to the theory of rheology of suspensions reducing the effects of excessive damping action of the Darcy-force as

$$F = 0.5 - \frac{1}{\pi} \arctan[100(g_l^{cr} - g_l)] \tag{8}$$

$$G = 0.5 + \frac{1}{\pi} \arctan[100(g_l^{cr} - g_l)]^{-4} \quad \text{where } g_l^{cr} = 0.5 \tag{9}$$

In the above equations, g_l^{cr} can be considered as a critical liquid fraction upto which the Carman–Kozeny equation remains valid.

Energy conservation:

$$\frac{\partial}{\partial t}(\rho T) + \nabla \cdot (\rho \vec{u} T) = \nabla \cdot \{(g_s \Gamma_s + g_l \Gamma_l) \nabla T\} - \frac{1}{c} \left[\frac{\partial}{\partial t}(\rho g_l \Delta H) + \nabla (\rho \vec{u} \Delta H) \right] \tag{10}$$

where $\Gamma_k = k_{Tk}/c_k$, and ΔH is the latent enthalpy.

Conservation of species:

The general species conservation equation can be written as

$$\frac{\partial}{\partial t}(\rho C_l) + \nabla \cdot (\rho \vec{u} C_l) = \nabla \cdot (D^+ \nabla C_l) + S_c \tag{11}$$

where D^+ is the mass diffusion coefficient and S_c is the source term. This general form assumes any special form depending on the microstructure under consideration. For non-equilibrium solidification represented by a columnar dendritic model with distinct microstructure, we have [3],

$$D^+ = \rho(g_s D_s k_p + g_l D_l) \quad \text{and} \quad S_c = \frac{\partial}{\partial t}[\rho g_s C_l] - k_p C_l \frac{\partial}{\partial t}(\rho g_s) \tag{12}$$

The boundary conditions consistent with the above set of differential equations are as follows:

$$\text{(a) Left wall: } u = 0,\ v = 0,\ T = T_{cold}(t),\ \partial C_l/\partial x = 0 \tag{13}$$

$$\text{(b) Right wall: } u = 0,\ v = 0,\ T = T_{hot}(t),\ \partial C_l/\partial x = 0 \tag{14}$$

$$\text{(c) Top wall: } u=0,\ v=0,\ \partial T/\partial y=0,\ \partial C_{\mathrm{l}}/\partial y=0 \tag{15}$$

$$\text{(d) Bottom wall: } u=0,\ v=0,\ \partial T/\partial y=0,\ \partial C_{\mathrm{l}}/\partial y=0 \tag{16}$$

The initial conditions appropriate to the physical situation are:

$$\text{at } t=0,\quad u=0,\quad T=T_{\mathrm{i}},\quad C_{\mathrm{l}}=C_{\mathrm{i}},\quad g_{\mathrm{l}}=1 \tag{17}$$

It can be noted here that in order to account for microscopic convection effects, the partition-coefficient (k_{P}) appearing in Equation (12) has to be appropriately modified, the numerical modelling and physical assessment of which is the basic objective of the subsequent discussion.

2.3. *Modification of partition-coefficient on account of solutal undercooling*

Common to many of the macroscopic solidification models using the lever rule or Scheil's equation [13] as the basis of microscopic solute conservation, there is an inherent assumption of a well-mixed solute in the liquid state. However, in practice, diffusivity in the liquid is finite, and there is an accumulation of solute at the liquid side of the interface within a diffusion (or solutal) boundary layer adjacent to the interface. This leads to a phenomenon commonly known as 'solutal undercooling', which may be described quantitatively as the difference between the interfacial and volume-averaged liquid species concentration. It can be noted here that the 'undercooling' is with respect to a change in local liquidus temperature as a result of change in species concentration in that location. However, transport in the liquid and in the solutal boundary layer adjacent to the liquidus front is influenced primarily by convection, which tends to decrease the solutal boundary layer thickness at the corresponding interface. It can be noted here that the solutal undercooling is expected to be a function of liquid species diffusivity, mean crystal and dendritic growth rate, mean thickness of the solutal boundary layer, the solid volume fraction, and the interfacial area concentration representing the interfacial geometry. Incorporation of such considerations in the macroscopic modelling is critically important, since the nature of the compositional boundary layer along the solid/liquid interface controls the distribution of solute in the other regions. This, in turn, determines the double-diffusive convection field, leading to a final macrosegregation pattern.

In order to implement this effect of solutal undercooling, we consider the solute profile (Figure 2) in the liquid for solidification with convection [13]. With the boundary condition of $C_{\mathrm{l}}=C_{\mathrm{l}}^{*}$ at the solid–liquid interface, and $C_{\mathrm{l}}=C_0$ at the edge of the diffusion boundary layer (for local equilibrium at the microscopic level), the solute distribution in the boundary layer is given by [13]

$$\frac{C_{\mathrm{l}}^{*}-C_{\mathrm{s}}^{*}}{C_0-C_{\mathrm{s}}^{*}}=\exp\left(\frac{R\delta}{D_{\mathrm{L}}}\right) \tag{18}$$

where R is the rate of interface movement, δ is the diffusion boundary layer thickness, and the superscript * denotes equilibrium condition.

Equation (18) can be used to define an effective partition coefficient, k_{p}', as the ratio of solid composition to bulk liquid composition, i.e.

$$k_{\mathrm{p}}'=\frac{k_{\mathrm{p}}}{k_{\mathrm{p}}+(1-k_{\mathrm{p}})\exp(-R\delta/D_{\mathrm{L}})} \tag{19}$$

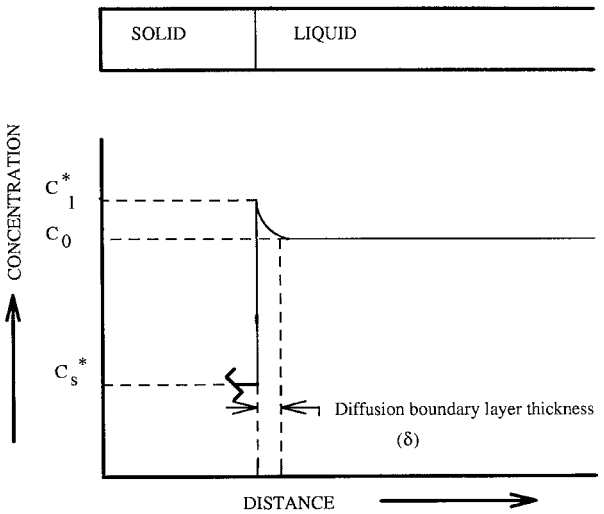

Figure 2. Formation of a diffusion boundary layer.

Such considerations in the context of crystal growth were originally made by Burton *et al.* [18], to account for solutal undercooling at the dendritic tip region (or, growth front). Equation (19) is of immense engineering use, since it relates the composition of solid forming in crystal growth to the alloy composition and growth conditions. Incorporation of Equation (19) into Scheil's equation [13] gives the so-called modified normal segregation equation. To visualize the physical effects of Equation (19), we consider two extreme cases. The first case corresponds to $R\delta/D_L \ll 1$. From Equation (19), this case reduces to $k'_p \to k_p$. Such a condition exists when the interfacial area concentration is large and the species diffusion length is small. Hence, solute in that region can be assumed to be well mixed in the liquid. The other limiting case corresponds to $R\delta/D_L \gg 1$, in which case, $k'_p \to 1$. This is true when the phase change occurs rapidly, solutal boundary layer is thick and/or diffusion rate is slow. All other cases in practice are intermediates of these two extremes. The manner in which this effect is numerically implemented will be described in detail in Section 3.

3. NUMERICAL MODELLING

3.1. Outline of basic steps

The basic framework of the present numerical method rests on a pressure based finite volume method according to the SIMPLER algorithm [19]. Accordingly, the governing equations are discretized by means of a fixed grid enthalpy based methodology. However, the algorithm is aptly modified to account for phase change considerations during non-equilibrium solidification on account of solutal undercooling. The broad steps of the numerical formulation are outlined in the flowchart presented in Figure 3. Only the special features of the numerical modelling, directly related with the focus of the present study will be discussed subsequently.

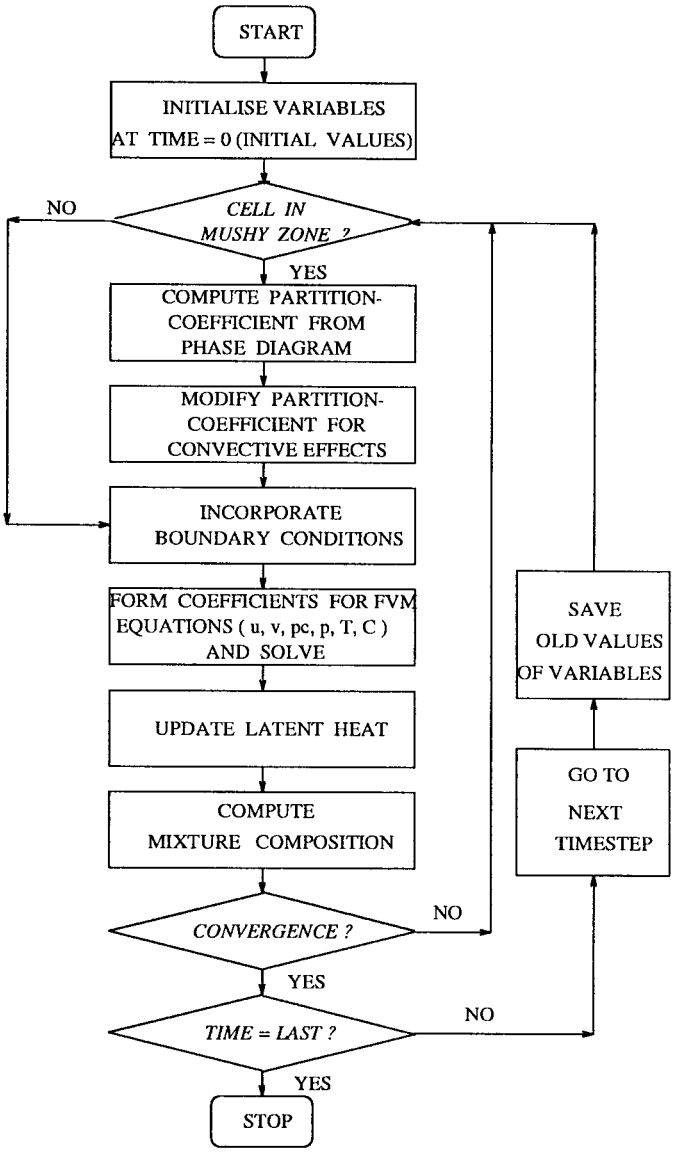

Figure 3. A flowchart of the numerical algorithm.

3.2. Numerical modelling of convection correction for partition coefficient

As mentioned in Section 2, the partition coefficient needs to be modified on account of solutal undercooling according to Equation (19). However, for an effective implementation in a macroscopic framework, the above expression has to be modelled in terms of macroscopically observable parameters. To achieve that purpose, we first recognize that the term $R\delta/D_l$ physically represents a ratio of advection to diffusion strengths associated with a phase-changing

control volume, which can be interpreted as a local solutal Peclet number (Pe). The advection strength, in this context, can be expressed as $R_{\mathrm{pc}}\Delta V/\Delta A$, where R_{pc} is the phase change rate per unit volume, ΔA is the solid–liquid interfacial area, and ΔV is the volume of the control volume. On the other hand, the diffusion strength may be expressed as $\rho D_{\mathrm{l}}/l_{\mathrm{ref}}$, where l_{ref} is the diffusion length scale in the liquid, characterizing mean species diffusion in the liquid adjoining the solid–liquid interface. The above may be combined to yield a macroscopic solutal Peclet number as

$$Pe_{\mathrm{macro}} = \frac{R_{\mathrm{pc}} l_{\mathrm{ref}}}{\rho_{\mathrm{s}} D_{\mathrm{l}} r} \tag{20}$$

where r is the interfacial area contraction (i.e. ratio of the solid–liquid interface area to the volume of the control volume), which characterises first-order geometric effects on interfacial species transfer.

In a control volume approach, the phase change rate per unit volume can be calculated by discretization of the following liquid-phase mass conservation:

$$\frac{\partial(g_{\mathrm{l}}\rho_{\mathrm{l}})}{\partial t} + \nabla\cdot(g_{\mathrm{l}}\rho_{\mathrm{l}}\bar{u}) = R_{\mathrm{pc}} \tag{21}$$

The transient term in Equation (21) is discretised using an implicit forward differencing scheme. The integrated convective source term is discretized by following an upwinding formulation as

$$\int_{C.V} \nabla\cdot(\rho_{\mathrm{l}} g_{\mathrm{l}}\bar{u})\,\mathrm{d}V = \text{flowout} - \text{flowin}$$

where

$$\text{flowin} = g_{\mathrm{l,W}}\max(F_{\mathrm{w}},0) - g_{\mathrm{l,P}}\max(-F_{\mathrm{w}},0) + g_{\mathrm{l,S}}\max(F_{\mathrm{s}},0) - g_{\mathrm{l,P}}\max(-F_{\mathrm{s}},0),$$

and

$$\text{flowout} = g_{\mathrm{l,P}}\max(F_{\mathrm{e}},0) - g_{\mathrm{l,E}}\max(-F_{\mathrm{e}},0) + g_{\mathrm{l,P}}\max(F_{\mathrm{n}},0) - g_{\mathrm{l,N}}\max(-F_{\mathrm{n}},0) \tag{22}$$

It can be noted that subscripts e, w, s, n, E, W, S, N in Equation (22) are in accordance with the usual nomenclature of control points in the context of description of a control volume in finite volume procedure, as sketched in Figure (4). 'F' in Equation (22) denotes the mass flow rate across the respective face of the control volume.

The diffusion length can be appropriately scaled as the ratio of mass diffusion coefficient of the liquid to the local growth velocity at the interface, in the context of dendritic growth. For such situations, macroscopic estimates of diffusion length can be made as

$$\frac{D_{\mathrm{l}}}{l_{\mathrm{ref}}} = \frac{|\vec{x}^{\,t} - \vec{x}^{\,t-\Delta t}|}{\Delta t} \tag{23}$$

where $\vec{x}$ represents location of the mushy-liquid interface and Δt is the time-step.
Also,

$$r = \frac{\sum_j A_{i,j}}{\sum_j \Delta V_{i,j}}, \quad \forall i \in (g_{\mathrm{l},i-1} \geqslant 0 \text{ and } g_{\mathrm{l},i+1} \leqslant 1) \tag{24}$$

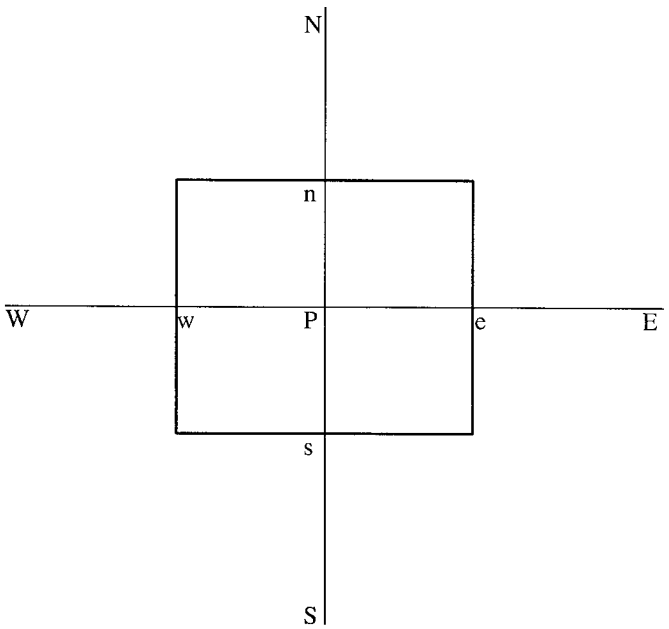

Figure 4. A typical computational control volume.

where $A_{i,j}$ is the area of phase changing interface pertaining to the control volume, $\Delta V_{i,j}$ the volume of the phase-changing control volume.

With the macroscopic estimates given by the discretized Equations (20)–(24), Equation (19) can now be conveniently utilized to obtain an effective partition-coefficient which accounts for solutal undercooling.

4. NUMERICAL RESULTS AND DISCUSSION

4.1. Model validation, selection of the solidifying system, and grid-independence study

For the purpose of validation of our numerical code, computations are first performed for the solidification of an aqueous ammonium chloride solution [2, 3], without incorporating any partition-coefficient correction. The numerical data used for this validation purpose are taken from Voller *et al.* [2]. This problem has been repeatedly used in the literature as a benchmark problem for binary alloy solidification. The results (not shown here) obtained using the present code compare excellently with those found in the literature [2, 3]. The validated code is then utilized to simulate the solidification of a Pb–Sn alloy in a rectangular enclosure (as shown in Figure 1). This system is specifically chosen for the following reasons:

1. Since the ratio of solutal to thermal buoyancy effect ($\beta_S \Delta C_l / \beta_T \Delta T$) is of the order of 10 for this system, an appreciable solutally driven convection can be expected inside the mushy region. The interaction of this convection with the thermally driven bulk fluid motion in the melt can result in an overall thermo–solutal (double-diffusive) convection

Table I. Table of Thermophysical properties [6].

Thermophysical properties	Sn 10 wt% Pb	Pb 15 wt% Sn
Specific heat (c)	250 J/kg	154.6 J/kg
Thermal conductivity of solid (k_s)	60 W/mK	34.97 W/mK
Thermal conductivity of liquid (k_l)	30 W/mK	17.8 W/mK
Density (ρ)	7000 kg/m^3	10100 kg/m^3
Viscosity (μ)	1.85×10^{-3} kg/ms	2.53×10^{-3} kg/ms
Liquid diffusion coefficient (D_L)	1×10^{-9} m^2/s	1×10^{-9} m^2/s
Latent heat of fusion (L)	5.9×10^4 J/kg	2.47×10^4 J/kg
Thermal expansion coefficient (β_T)	-8.75×10^{-5} K^{-1}	-1.23×10^{-4} K^{-1}
Solutal expansion coefficient (β_S)	0.525	-0.339
Eutectic temperature (T_E)	183°C	183°C
Eutectic concentration (mass fraction) (C_E)	0.391	0.619
Equilibrium partition coefficient (k_p)	0.0656	0.31

in which solutal buoyancy effects in the interdendritic melt play a significant role. It may be noted that the above ratio for a typical metal analogue system (say, ammonium chloride-water solution) is only of the order of unity, which is one order of magnitude less in comparison to the metallic system chosen.

2. Since the chosen system is a real metal-alloy system, the present simulation is expected to reveal various aspects of transport phenomena associated with a metallurgically relevant solidifying system. The solidification behaviour of such systems may be different from the response of metal analogs in similar situations, owing to a large difference in many of the thermophysical properties between them.
3. Due to relatively lower melting points associated with the alloy system, experimental results are abundantly available in the literature [16], with which the present simulation results can be compared.

Numerical simulations are performed for the following two cases of initial alloy composition:

Case I: Pb–15 wt% Sn

Case II: Sn–10 wt% Pb

The relevant thermophysical properties for the two alloys are listed in Table I. The physical data and boundary temperatures are taken in accordance with the experimental conditions reported in Reference [16]. The variations of boundary temperatures with time are shown in Figure (5), in accordance with Shahani *et al.* [16]. The size of the problem domain is taken as 0.1 m $\times$ 0.1 m.

A comprehensive grid-independence study is undertaken to determine the appropriate spatial discretization, temporal discretization and iteration convergence criteria to be used. The quantities examined in this study are the maximum magnitudes of the various scalar variables (horizontal and vertical velocity component, temperature, solute concentration in the liquid, the liquid mass fraction), the interface location and its growth rate. As an outcome of this study, we have taken a 80×80 non-uniform grid as our final simulation matrix, with very fine grids along the x-direction near the cold wall ($\sim$0.05 mm). Also, we have adopted a gradually increasing time step, starting from an initial value of 0.1 s to a final value of 1 s for

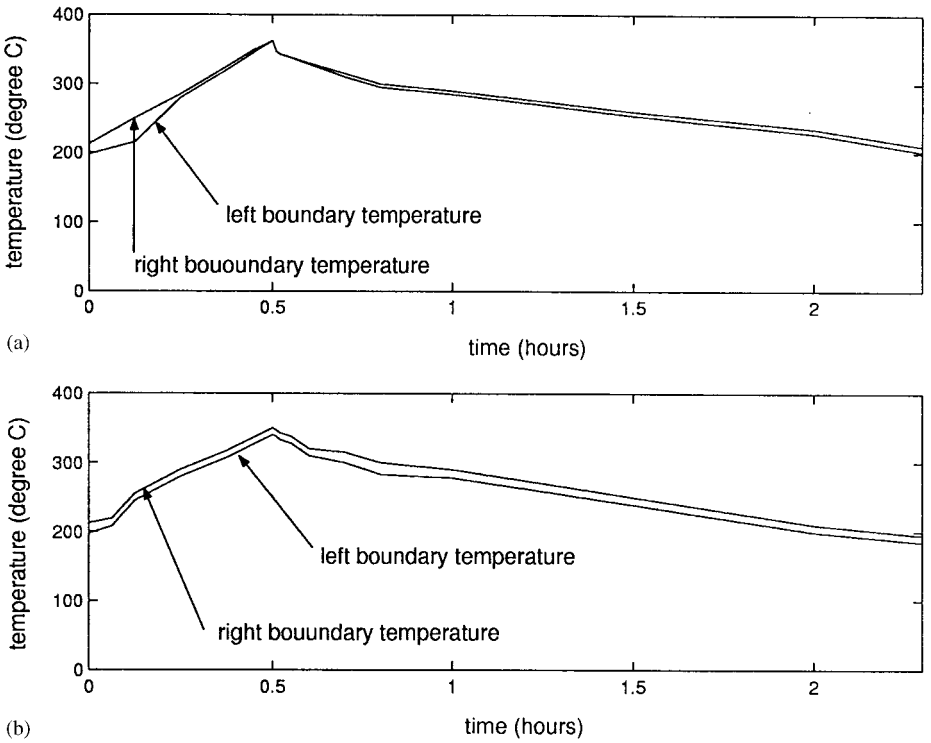

Figure 5. Variation of boundary temperature with time for (a) Sn 10 wt% Pb alloy and (b) Pb wt% Sn alloy.

the later stages. Selection of such gridding and time step is primarily meant to capture the initial transients, as the solidification begins. Also, small time-steps ensure that the predictions regarding the interface growth rates are accurate enough. However, it is found that, a finer grid system and time step size is unable to alter the results appreciably.

Convergence in inner iterations is declared only when the following conditions are simultaneously satisfied:

(i) $|(\phi - \phi_{\text{old}})/\phi_{\max}| \leqslant 10^{-4}$, where ϕ stands for each variable u, v, T, and C_l at a grid point at the current iteration level, ϕ_{old} represents the corresponding value at the previous iteration level, and $\phi_{\max}$ is the maximum value of the variable at the iteration level in the entire domain.

(ii) Absolute values of the energy balance are within 0.1% of the total stored energy within the computational domain.

4.2. Results for Case I

4.2.1. Double diffusive convection. Figure (6) shows the convection pattern for the case I (Pb–15 wt% Sn), at time = 10 min after commencement of solidification. The streamlines show the evolution of a minor vortex due to solutal buoyancy effects near the left bottom corner of the cavity. The development of this minor vortex is due to solutal gradient build-up

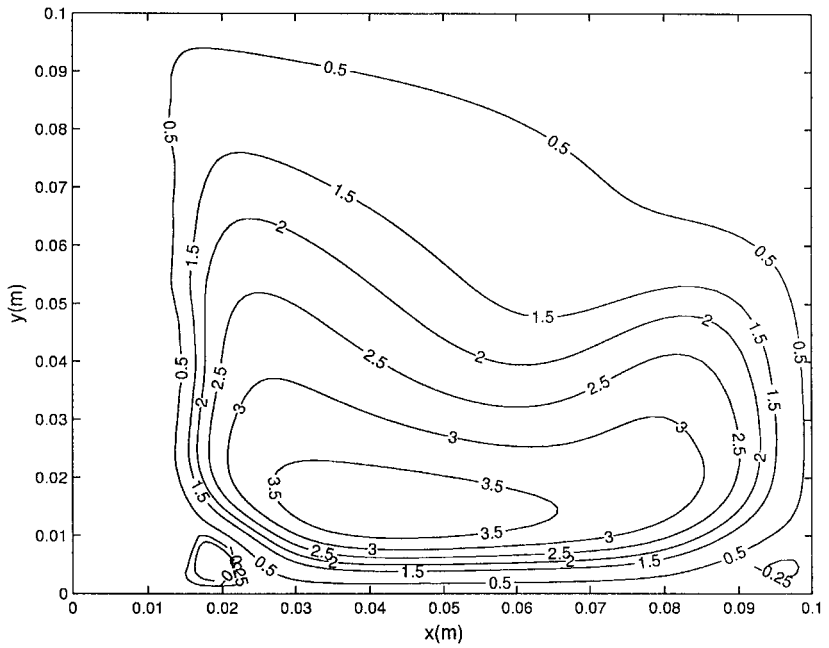

Figure 6. Stream function plots at time = 10 min for Pb 15 wt% Sn alloy.

caused by the transportation of solute from the mush by the thermal buoyancy driven major vortex. To illustrate these effects clearly, the corresponding portion of the cavity is zoomed in Figure (7), where the counteracting effects in the velocity vectors can be clearly observed. It can be noted that thermal and solutal buoyancy effects oppose each other for the nominal composition of 15 wt% Sn in the alloy. As solidification proceeds, Sn is rejected into the liquid, which is lighter than the solvent (Pb) and hence tends to move up. On the other hand, thermal buoyancy effects tend to push the fluid down the phase-changing interface, on account of localized cooling effects due to rejection of latent heat during solidification. Presence of localized solutal convection is seen only in those portions of the cavity in which the solutal buoyancy effect is strong enough to completely overcome the thermal convection. In other locations, solutal buoyancy reduces the strength of the flow-field created by thermal buoyancy.

4.2.2. Effect of solutal undercooling on convection. Figures (8)–(10) exhibit the final macrosegregation pattern at different vertical sections of the cavity, whereas Figure (11) shows the same at a horizontal location of the cavity. In each of these figures, the results obtained by the present model are compared with the experimental observations [16] and with the corresponding numerical ones obtained without the convection–correction of partition-coefficient.

From Figures (8)–(10), it is evident that there is a positive macrosegregation near the top of the cavity, and a negative macrosegregation in the rest of the cavity. Here, a positive macrosegregation implies that solute concentration is greater than that of the nominal alloy composition (15% Sn, in this case). It may be noted here that solute is rejected into the liquid throughout the mushy region. However, as evident from Figure (7), there is a net upward

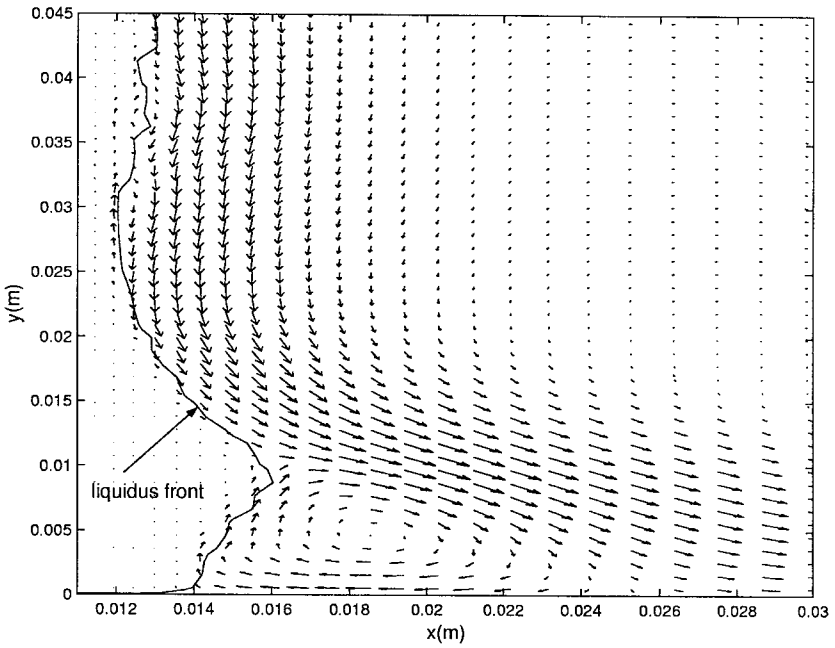

Figure 7. Velocity vectors at a zoomed location near the cavity bottom at time = 10 min for Pb 15 wt% Sn alloy.

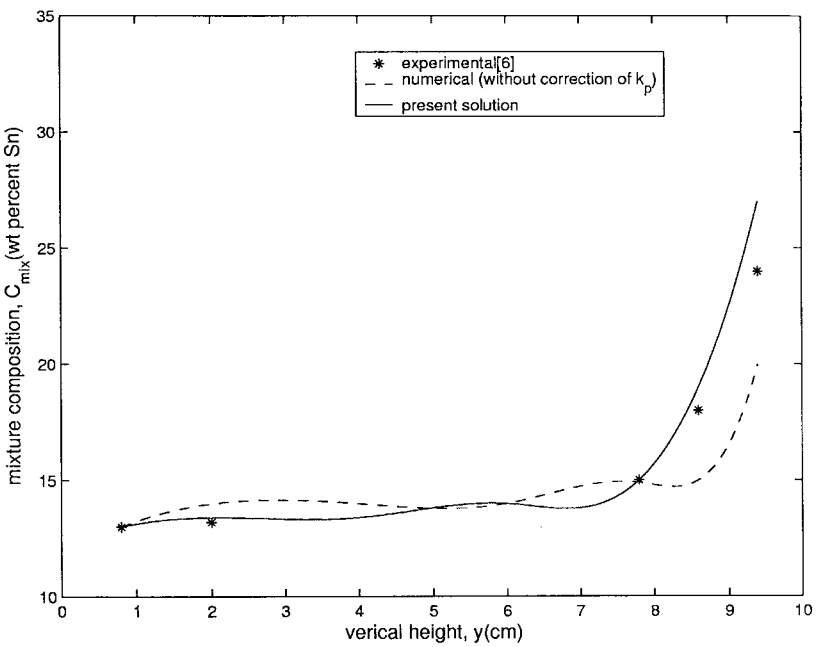

Figure 8. Final macrosegregation for Pb 15 wt% Sn alloy at $x = 3.5$ cm.

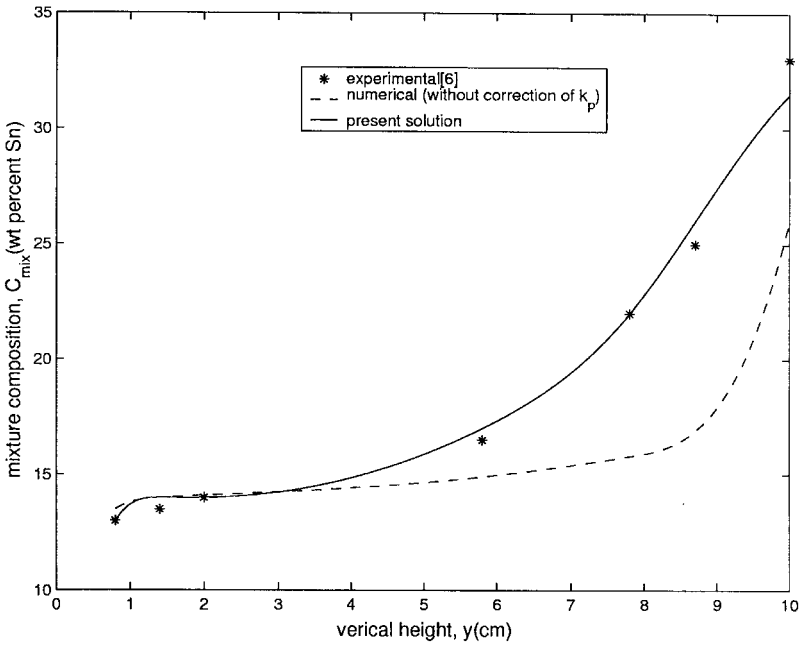

Figure 9. Final macrosegregation for Pb 15 wt% Sn alloy at $x = 8$ cm.

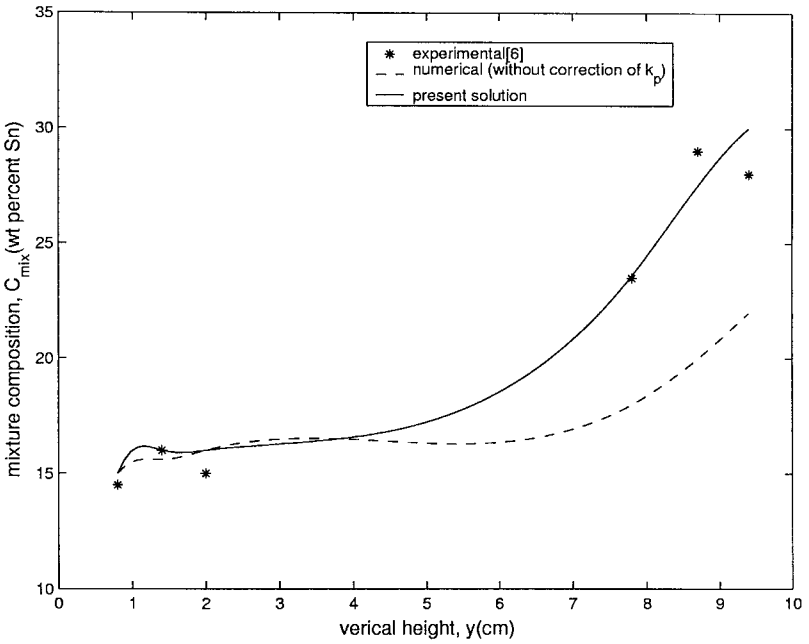

Figure 10. Final macrosegregation for Pb 15 wt% Sn alloy at $x = 9.47$ cm.

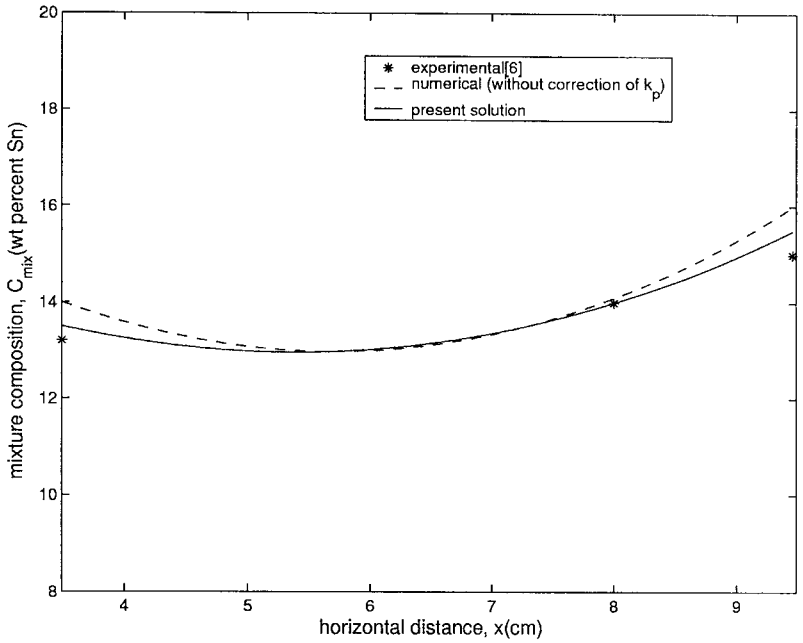

Figure 11. Final macrosegregation for Pb 15 wt% Sn alloy at $y = 2$ cm.

thermosolutal flow close to the phase changing front inside the mushy region. This leads to an accumulation of solute near the top of the cavity inside the mushy region, at the cost of depletion of solute in the bottom portion. The composition of the final solidified macrostructure at any location of the cavity is determined by the instantaneous solute concentration adjacent to the solidification front during the evolution of the phase change process.

It is clearly evident from Figures (8)–(10) that results from the numerical simulation incorporating solutal undercooling effects (present model) are distinctly closer to the experimental results, as compared to the model predictions without the inclusion of solutal undercooling effects (i.e. no correction of k_p). These results imply that the present model predicts the amount of solute segregation more accurately. This can be physically explained as follows: when the solutal undercooling effects are not considered, the fluid flow inside the mushy region is predominantly influenced by the global double-diffusive convection effects. However, with the present model, on account of solute build-up at the dendritic tips, there is an additional strength of solutal convection, which can be scaled as $\{g(C_t - C_0)D_l/RC_0\}^{0.5}$, where C_t is the species concentration at the dendritic tip, C_0 is the nominal alloy composition, D_l is the diffusivity of solute in the liquid, and R is the interface speed. The basis of this expression is the estimation of a solutal Grashoff number [20], where the characteristic distance is best represented by D_l/R. This additional strength of solutal convection transports the solute more effectively towards the top of the cavity adjacent to the phase-change front, leading to an enhanced final macrosegregation, as predicted by the present model.

Figure (11) shows the variation of species composition in the horizontal direction in the final macrostructure at a height of 2 cm from the bottom of the cavity. It is observed that the variation of species composition in the horizontal direction is not very significant. This is

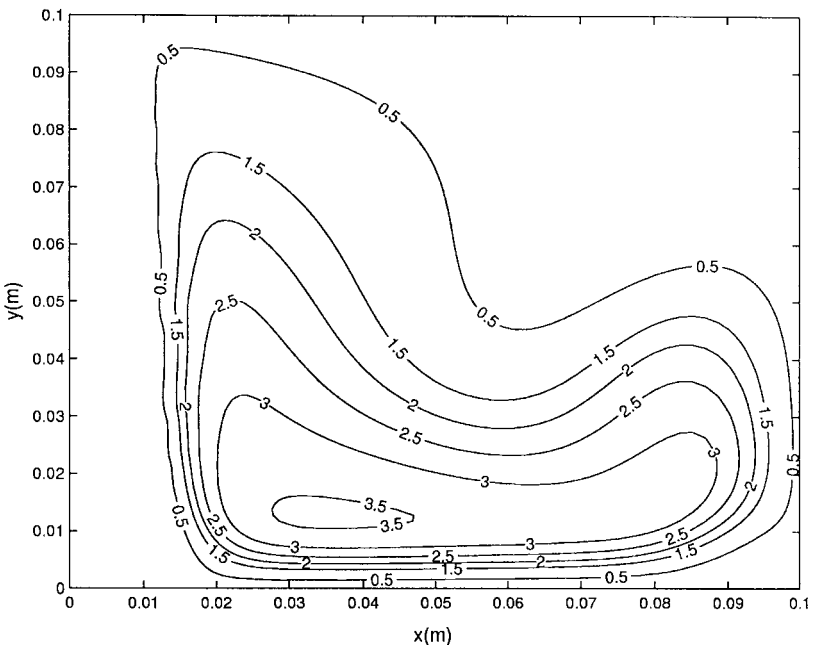

Figure 12. Stream function plots at time = 10 min for Sn 10 wt% Pb alloy.

because convection is much weaker in the horizontal direction than in the vertical direction in the layer adjacent to the phase changing front inside the mushy region.

4.3. Results for Case II

4.3.1. (a) Double diffusive convection. Figure (12) shows the convection mode for Case II (Sn-10 wt% Pb), at time = 10 min after solidification begins. Unlike in the previous case, no minor vortex appears. This is confirmed by the zoomed figure (Figure 13), showing the velocity vectors in the same portion of the cavity as depicted by Figure (7) for the previous case. This phenomenon can be attributed to the fact that as the heavier solute (Pb) is rejected into the liquid upon solidification, it tends to create a downward flow on account of density variations across the phase changing front. This flow aids the thermal buoyancy driven flow originated as a result of cooling effect at the solidifying interface. Thus, the resultant double diffusive flow creates only a major unidirectional counterclockwise rotating vortex.

4.3.2. (b) Effect of solutal undercooling on convection. Similar to Case I, we have plotted the species composition variation at different sections of the cavity, and the results are shown in Figures (14)–(17). In this case, the solutal buoyancy aids thermal buoyancy, resulting in a strong downward thermo-solutal convection inside the mushy region. Hence there is an accumulation of the heavier solute (Pb) near the bottom of the cavity, at the expense of solute depletion in the upper portion of the cavity. This explains the occurrence of positive macrosegregation of solute near the bottom in the final macrostructure of the solidified cavity, as observed in the figures. In this case, too, we find that the predictions from the present model

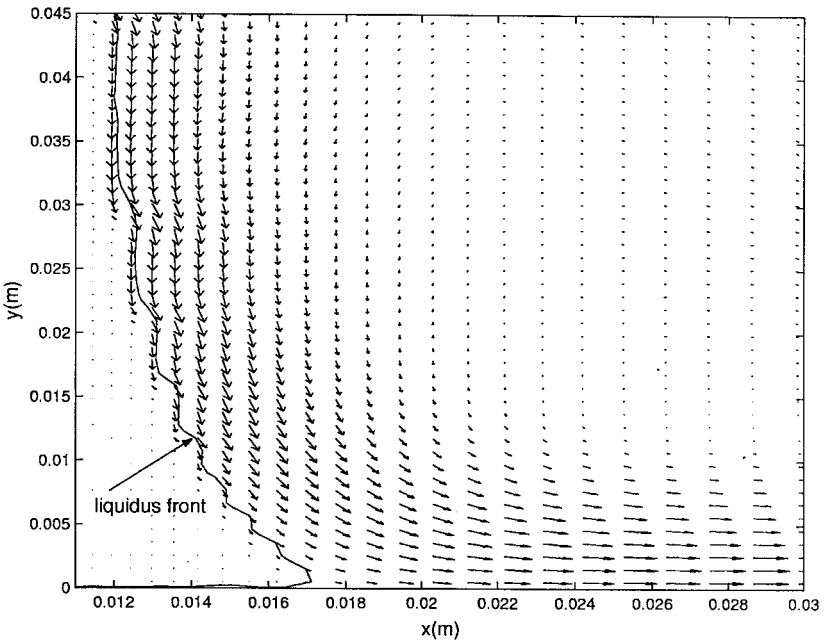

Figure 13. Velocity vectors at a zoomed location near the cavity bottom at time = 10 min for Sn 10 wt% Pb alloy.

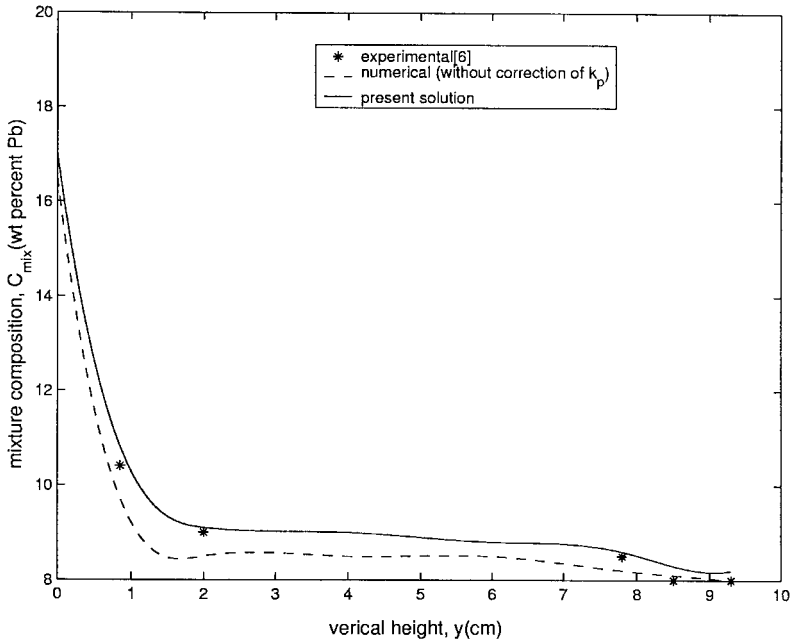

Figure 14. Final macrosegregation for Sn 10 wt% Pb alloy at $x = 3.5$ cm.

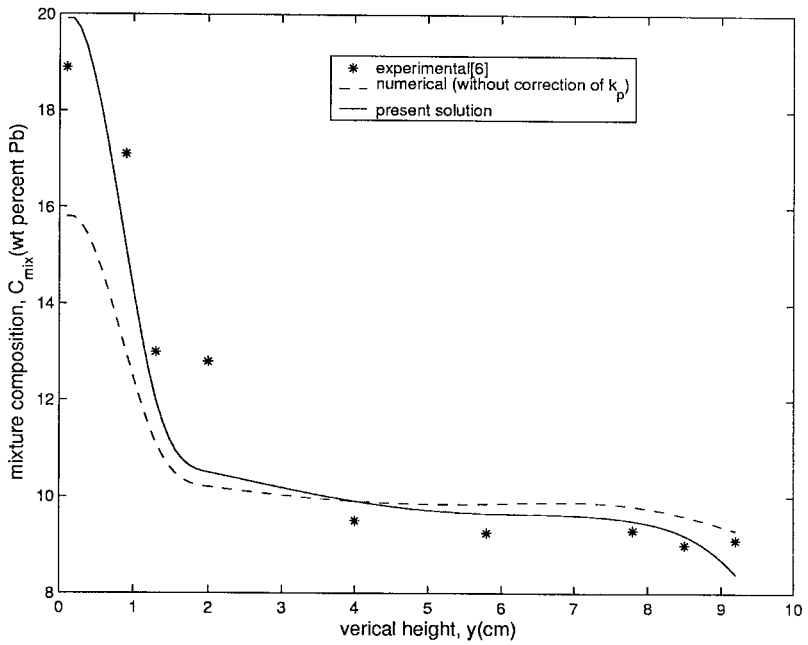

Figure 15. Final macrosegregation for Sn 10 wt% Pb alloy at $x = 8$ cm.

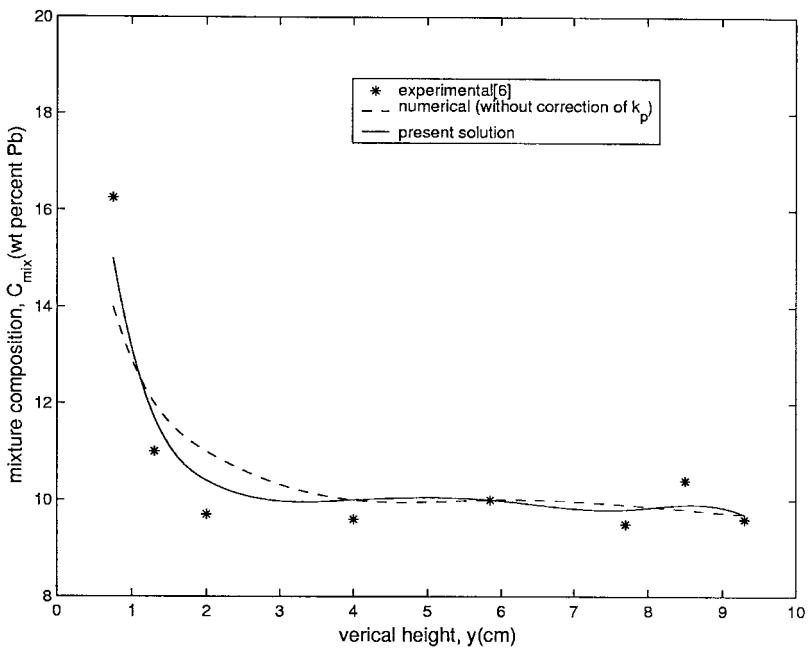

Figure 16. Final macrosegregation for Sn 10 wt% Pb alloy at $x = 9.47$ cm.

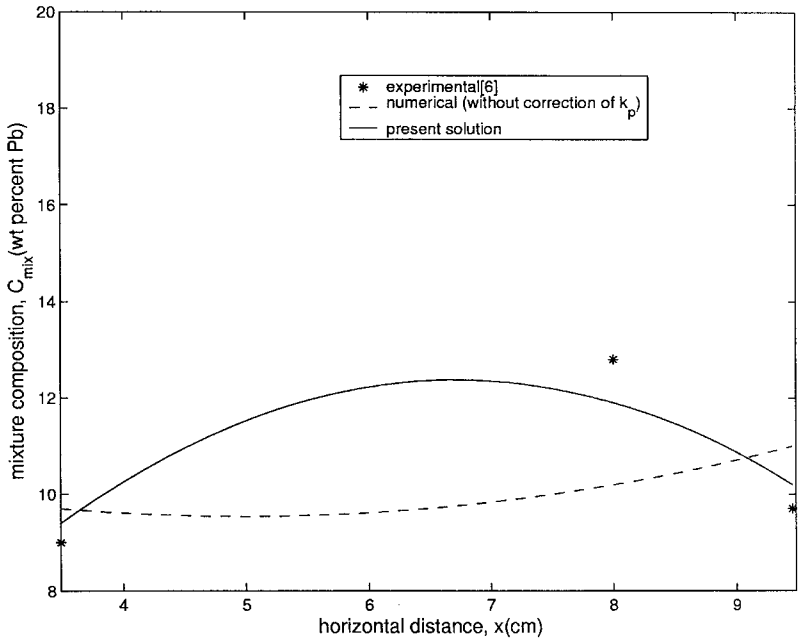

Figure 17. Final macrosegregation for Sn 10 wt% Pb alloy at $y = 2$ cm.

agrees with the corresponding experimental results better than the case without considering solutal undercooling. The explanation is similar to that in Case I.

5. CONCLUSIONS

We have developed a macroscopic model for double diffusive convection during alloy solidification, which takes into account the non-equilibrium effects due to solutal undercooling. Such an effect arising from microscopic convection near the diffusion boundary layer adjacent to the mushy region is captured by devising a macroscopic numerical model based on a fixed-grid, enthalpy-based, control volume approach. In the present model, microscopic features pertaining to solutal undercooling are incorporated through a 'convection-correction' of the partition-coefficient by means of a number of macroscopically observable parameters. This is distinctly different from the treatments in the corresponding micro–macro models in the sense that the present model does not involve any explicit microscopic parameters, which are normally difficult to resolve in macroscopic length scales. Numerical simulations are performed for a two-dimensional transient solidification of Pb–Sn alloys in a rectangular cavity, corresponding to both hypoeutectic and hpereutectic initial composition. The simulation results are compared with the corresponding experimental observations quoted in the literature, and an excellent agreement can be obtained. From these results, it can be concluded that non-equilibrium effects on account of solutal undercooling can result in an enhanced macrosegregation.

APPENDIX A

Nomenclature

A_μ	A constant in the Darcy source term
$A_{i,j}$	area of phase changing interface pertaining to a computational control volume
$a_\mathrm{p}, a_\mathrm{p}^0$	coefficients in discretization equation
C	species concentration
c	specific heat
D	mass diffusion coefficient of the species
F	a constant in Darcy source term/mass flow rate across a control volume face
G	a constant in the Darcy source term
g	volume fraction(when subscripted)/acceleration due to gravity(when unsubscripted)
ΔH	latent enthalpy
k	thermal conductivity
k_p	partition coefficient
K	porosity constant
L	latent heat of fusion
l_ref	diffusion length in the liquid
p	pressure
q	heat flux
Pe	Peclet number
R	interface speed
R_pc	phase change rate per unit volume
r	interfacial area concentration
S	source term
T	temperature
t	time
Δt	size of the time step
u	x component of velocity
v	y component of velocity
$\vec{u}$	velocity vector
X, Y	dimensions of the cavity
x, y	co-ordinate variables
$\vec{x}$	location of the mushy-liquid interface

Greek symbols

β_S	solutal expansion coefficient
β_T	thermal expansion coefficient
δ	diffusion boundary layer thickness
ϕ	general scalar variable
λ	relaxation factor
μ	dynamic viscosity
ρ	density

Subscripts

cold	cold wall
E	eutectic/grid point located at 'east' of a typical control volume
i	initial
hot	hot wall
L	liquidus
l	liquid phase
m	evaluated at melting point
macro	macroscopic
N	grid point located at 'north' of a typical control volume
ref	reference
S	grid point located at 'south' of a typical control volume
s	solid phase
t	related to the dendritic tip
old	old iteration value
W	grid point located at 'west' of a typical control volume
0	nominal

Superscript

t	corresponding to the time level 't'
$'$	modified
*	equilibrium

REFERENCES

1. Bennon WD, Incropera FP. A continuum model for momentum, heat and species transport in binary solid–liquid phase change system—I. Model formulation. *International Journal of Heat and Mass Transfer* 1987; **30**:2161–2170.
2. Bennon WD, Incropera FP. A continuum model for momentum, heat and species transport in binary solid–liquid phase change systems—II. Application to Solidification in a rectangular cavity. *International Journal of Heat and Mass Transfer* 1987; **30**:2171–2187.
3. Voller VR, Brent AD, Prakash C. The modeling of heat, mass and solute transport in solidification systems. *International Journal of Heat and Mass Transfer* 1989; **32**:1719–1731.
4. Brody HD, Flemings MC. Solute redistribution in dendritic solidification. *Transactions of the Metallurgical Society of AIME* 1966; **236**:615–624.
5. Clyne TW, Kurz W. Solute redistribution during solidification with rapid solid state diffusion. *Metallurgical Transactions* 1981; **12A**:965–971.
6. Ohanka I. Mathematical analysis of solute redistribution during solidification with diffusion in solid phase. *Transactions of the Iron and Steel Institute of Japan* 1986; **26**:1045–1051.
7. Kobayashi S. Solute redistribution during solidification with diffusion in solid phase: a theoretical analysis. *Journal of Crystal Growth* 1988; **88**:87–96.
8. Ogilvy AJW, Kirkwood DH. A model for the numerical computation of microsegregation in alloys. *Applied Scientific Research* 1987; **44**:43–49.
9. Roosz A, Gacsi Z, Fuchs EG. Solute redistribution during solidification and homogenization of binary solid solution. *Acta Metallurgica* 1984; **32**:1745–1754.
10. Battle TP, Pehlke RD. Mathematical modeling of microsegregation in binary metallic alloys. *Metallurgical Transactions B* 1990; **21B**:357–375.
11. Kraft T, Chang YA. Predicting microstructure and microsegregation in multicomponent alloys. *Journal of Metals* 1997; **49**:20–28.
12. Voller VR, Beckermann C. A unified model of microsegregation and coarsening. *Metallurgical Transactions A* 1999; **30A**:2183–2189.

13. Flemings MC. *Solidification Processing*. McGraw Hill: New York, 1974; 34–44.
14. Rappaz M. Modelling of microstructure formation in solidification processes. *International Materials Review* 1989; **34**:93–123.
15. Flemings MC. Solidification Processing. In *Materials Science and Technology*, Cahn RW, Hassen P, Kramer EJ (eds), vol. 15. VCH, New York; 1991, 1–56.
16. Shahani H, Amberg G, Fredriksson H. On the Formation of Macrosegregations in Unidirectionally Solidified Sn–Pb and Pb–Sn alloys. *Metallurgical Transactions* 1992; **23A**:2301–2311.
17. Morvan D, Ganaoui M El, Bonboux P. Numerical simulation of a 2-D crystal growth problem in vertical Bridgman–Stockbarger furnace: Latent heat effect and crystal-melt interface morphology. *International Journal of Heat and Mass Transfer* 1999; **42**:573–579.
18. Burton JA, Prim R, Slichter W. The distribution of solute in crystal growth from the melt. Part 1. *Theoretical Journal of Chemical Physics* 1953; **21**(11):1987–1991.
19. Patankar SV. *Numerical Heat Transfer and Fluid Flow*. Hemisphere/McGraw-Hill: Washington, 1980.
20. Pimputkar SM, Ostrach S. Convection effects in crystal growth from melt. *Journal of Crystal Growth* 1981; **55**:614–646.

